processes

MDPI

Article

Reservoir Dynamic Reserves Characterization and Model Development Based on Differential Processing Method: Differentiated Development Strategies for Reservoirs with Different Bottom Water Energies

Hongwei Song [1], Shiliang Zhang [1], Feiyu Yuan [1], Lu Li [1], Yafei Fu [1], Chao Yu [1] and Chao Zhang [2,*]

[1] Sinopec Northwest Oilfield Company, Urumqi 830011, China; songhw.xbsj@sinopec.com (H.S.); zhangshil.xbsj@sinopen.com (S.Z.); yuanfy.xbsj@sinopec.com (F.Y.); lilu.xbsj@sinopec.com (L.L.); fuyaf123.xbsj@sinopec.com (Y.F.); cyu13142@gmail.com (C.Y.)
[2] School of Petroleum Engineering, China University of Petroleum (East China), Qingdao 266580, China
* Correspondence: zhangc@upc.edu.cn

Abstract

Complex carbonate reservoirs feature large-scale karst cavern structures, exhibiting complex pore and bottom water energy distributions, which increase the difficulty of reservoir development and require targeted research. This paper proposes a new method for dynamic reserves calculation in these reservoirs based on the Differential Processing Method (DPM) and aimed at optimizing the development of complex reservoirs. The AD22 unit of the Tarim Oilfield in Xinjiang is taken as the research object, and this reservoir features complex karst and fault characteristics, which traditional reserves calculation methods cannot effectively capture due to its complex heterogeneous distribution. This study constructs a refined reservoir numerical model through 3D geological modeling and impedance inversion techniques, calculates dynamic reserves using the DPM, and compares the result with traditional material balance and production data analysis methods. The results indicate that the DPM has an advantage in estimating the petrophysical parameters and reserve utilization in such reservoirs. The error between the constructed reservoir numerical model and the actual reservoir development historical data is only 2.04%, demonstrating a good reference value. The model shows that more than 60% of the recoverable reserves in the target unit are located in areas shallower than 160 m underground, while the current development degree is only 12.6%. The model shows that the recovery rate is low in the strong bottom water energy areas of the unit, while the recovery potential is high in the weak bottom water areas. Therefore, a differentiated development strategy based on varying bottom water energy is required to enhance development efficiency. The model indicates that this strategy can improve the comprehensive development benefits of the reservoir by 81.66% over the existing baseline, demonstrating significant potential. This study provides new ideas and methods for dynamic reserve estimation and development strategy optimization for complex carbonate reservoirs, verifies the effectiveness of the DPM in evaluating the development of complex bottom water energy reservoirs, and offers data references for related research and field applications.

Keywords: fractured-vuggy reservoir; reservoir numerical simulation; differential processing method

check for updates

Academic Editor: Qingbang Meng

Received: 1 May 2025
Revised: 4 June 2025
Accepted: 20 June 2025
Published: 28 June 2025

Citation: Song, H.; Zhang, S.; Yuan, F.; Li, L.; Fu, Y.; Yu, C.; Zhang, C. Reservoir Dynamic Reserves Characterization and Model Development Based on Differential Processing Method: Differentiated Development Strategies for Reservoirs with Different Bottom Water Energies. *Processes* **2025**, *13*, 2053. https://doi.org/10.3390/pr13072053

Copyright: © 2025 by the authors. Licensee MDPI, Basel, Switzerland. This article is an open access article distributed under the terms and conditions of the Creative Commons Attribution (CC BY) license (https://creativecommons.org/licenses/by/4.0/).

1. Introduction

With the continuous growth of global energy demand and the advancement of oil and gas exploration and development technologies, reservoir modeling and dynamic reserve calculation have emerged as critical research directions in petroleum exploration, providing essential data references and theoretical guidance for optimizing development strategies of target reservoirs [1–3]. Complex carbonate reservoirs exhibit high heterogeneity and complex geological characteristics, attributed to the presence of numerous structures such as fractures, karst caverns, faults, and folds, often accompanied by complex sedimentary layering. Under these conditions, the distribution of bottom water energy and fluid permeability shows erratic variations, with significant structural complexity and heterogeneity. Due to their unique geological evolution processes and structural distribution features, advancing development and predicting the development outcomes become challenging. Under conventional development models, oil and gas extraction is difficult, leading to low ultimate recovery rates [4–6]. Consequently, efficient modeling and precise dynamic reserve calculation methods tailored to such reservoirs have become pivotal for enhancing hydrocarbon development outcomes and recovery rates. Dynamic reserve calculation refers to the process of dynamically assessing oil and gas reserves by combining real-time development data (such as pressure, production, and water–oil ratio) monitored from the target oilfield with geological models. Unlike conventional static reserve estimation, which can only output development status data for a fixed time period, dynamic reserve calculation reflects the changes in various reservoir property parameters throughout the entire development process [7–11]. Additionally, this study takes into account the influence of factors such as bottom water energy, gas cap, and water invasion, enabling more accurate predictions of the target reservoir's recoverable reserves, recovery rates, and future development potential. Dynamic reserve calculation typically uses techniques such as numerical simulation, material balance, and production data analysis to analyze the reservoir's extraction process and provide a basis for optimizing the oil and gas field development plan [12–16]. The Differential Processing Method (DPM), as an innovative dynamic reserve calculation technique, demonstrates superior applicability in characterizing parameters of complex fractured–vuggy reservoirs with unique edge/bottom water distribution patterns. By incorporating rock compressibility variations, dynamic adjustments of formation pressure, and water encroachment effects, DPM enables accurate quantification of bottom water energy, oil–water displacement efficiency, and water invasion processes. This method proves particularly vital in reservoirs with strong bottom water support, effectively mitigating estimation errors inherent to traditional approaches [14,17–19]. The key to establishing this model lies in inputting the changes in various parameters of the target block's strata over development time into the software, and performing a more refined grid-based modeling of the overall structure [20–23].

The AD22 unit, located in the Tarim Oilfield of Xinjiang, serves as a typical complex carbonate reservoir unit in Block 12 of the Tahe oil region. It is characterized by complex karst dissolution, bottom water energy distribution, and fault features, with particularly significant reservoir heterogeneity. Dominated by dissolution cavities, pores, and fractures as primary reservoir spaces, its development patterns significantly differ from conventional sandstone reservoirs [24–26]. Traditional methods, including material balance and conventional dynamic reserve calculation techniques, fail to meet the requirements for precise characterization of the AD22 unit. Therefore, this study proposes the Differential Processing Method for dynamic reserve calculation based on karst development patterns and reservoir space heterogeneity, with comparative validation against material balance methods and production data analysis to demonstrate its advantages in complex carbonate reservoir development. In this study, detailed geological analysis of the AD22 unit first identifies the

reservoir's key characteristics and heterogeneity distribution. Subsequently, 3D geological modeling technology integrated with acoustic impedance inversion and dynamic data constraints establishes a refined reservoir architecture [27–29]. The DPM is then applied for dynamic reserve calculation, analyzing reserve drainage efficiency across different bottom water energy zones and proposing differentiated development optimization strategies. The results indicate that reserve development in the AD22 unit is significantly influenced by bottom water energy; strong bottom water zones exhibit lower recovery efficiency, while weak bottom water zones demonstrate higher recovery potential [30–32].

This study proposes a new method for dynamic reserve calculation suitable for complex carbonate reservoirs, known as the Differential Processing Method (DPM). Based on this method, a high-accuracy reservoir development model was established, and the effectiveness of this approach in evaluating the development performance of reservoirs with varying bottom water energy levels was validated. Through comparative analysis with conventional methods, the research demonstrates DPM's superior capabilities in precise reserve evaluation and recovery rate enhancement. The findings establish a scientific basis for subsequent efficient development of target reservoir units while providing strategic optimization references for analogous reservoir developments.

2. Experimental Section

2.1. Reservoir Model Construction

In oilfield development processes, the precise construction of reservoir models is critical for reservoir management and dynamic reserve evaluation. Particularly in complex carbonate reservoirs characterized by heterogeneity, fracture networks, and karst features, traditional static reserve assessment methods prove inadequate for accurate petrophysical characterization. This study establishes a refined reservoir numerical simulation model through the integration of karst evolution mechanisms, fracture-controlled numerical simulation methods, 3D geological modeling, and dynamic reservoir development data constraints using the tNavigator v22.3 geological modeling software as the medium. This methodology enables comprehensive characterization and dynamic analysis of complex reservoir systems.

The target reservoir of this study is the carbonate reservoir in the AD22 unit of the Tarim Oilfield, Xinjiang, China. Based on existing data including core analysis, geological logs, and well logging profiles, detailed geological characterization was conducted to identify the reservoir's principal lithological components, pore structures, and spatial distribution characteristics of fractures and vugs. Subsequent reservoir modeling employed a compartmentalized hierarchical approach, where the AD22 unit was subdivided into multiple secondary reservoir compartments. Each compartment underwent meticulous calibration using key parameters including lithology, porosity, and permeability. The reservoir petrophysical parameters of each well group in the target unit are shown in Table 1. To enhance modeling precision, 3D geological modeling techniques were implemented, with customized parameter assignments (e.g., vug-dominant, fracture-dominant, matrix-dominant) executed sequentially for each secondary compartment according to reservoir heterogeneity. This methodology ensures accurate spatial characterization of reservoir properties and internal fluid dynamics. Acoustic impedance inversion technology was further integrated to synthesize seismic exploration data with geological models. This technique generated refined reservoir distribution insights, particularly enhancing parameter resolution in reservoir zones where conventional measurements prove challenging. The impedance parameters derived from production wells in the target reservoir unit are systematically cataloged in Table 2.

Table 1. The reservoir petrophysical parameters of each well group in the target unit.

Unit	Associated Fracture-Vug System	Average Permeability/(mD)	Average Porosity/(%)	Average Production Oil Water Cut/(%)	Average Gas-to-Oil Ratio/(m^3/m^3)	Average Productivity Index (bbl/psi/Day)	Reservoir Rock Type	The Presence of a Gap Cap.
AD22 Unit	AD22 Well Cluster	1526.38	17.93	52.26	66.24	4.39	carbonate rock	Yes
	TH12208 Well Cluster	1824.74	15.84	42.09	70.25	1.96	carbonate rock	Yes
	TH12201 Well Cluster	1833.09	11.01	67.9	73.64	2.28	carbonate rock	Yes
	TH12332 Well Cluster	1806.17	13.64	36.7	45.93	2.12	carbonate rock	No

Table 2. Acoustic impedance statistics of wells in the target reservoir unit.

Well Number	Acoustic Impedance/ ($\times 10^7$)	Well Number	Acoustic Impedance/ ($\times 10^7$)	Well Number	Acoustic Impedance/ ($\times 10^7$)
1	1.33	13	1.36	25	1.33
2	1.41	14	1.39	26	1.45
3	1.36	15	1.36	27	1.38
4	1.39	16	1.35	28	1.43
5	1.31	17	1.23	29	1.38
6	1.44	18	1.32	30	1.47
7	1.36	19	1.40	31	1.46
8	1.35	20	1.51	32	1.42
9	1.41	21	1.42	33	1.51
10	1.30	22	1.53	34	1.48
11	1.49	23	1.41		
12	1.38	24	1.38		

By integrating existing reservoir data, an initial framework model for the distribution of vuggy reservoir bodies was established, using an acoustic impedance and structural tensor attribute fusion modeling approach to characterize continuously developed vuggy reservoir bodies. To further improve the accuracy of the model and better characterize karst-controlled reservoirs, we incorporated vug size distribution data from individual reservoir bodies into the framework model, as shown in Table 3. Specifically, we conducted on-site collection and measurement of porosity and vug size for different reservoir units to obtain the vug size distribution data within each reservoir body. Then, by performing statistical analysis on these data, we constructed a probability model for the vug size distribution and integrated this model as an input parameter into the reservoir body distribution framework model to ensure the continuity and spatial consistency of vug distribution. Through this process, we not only considered the vug characteristics of individual reservoir bodies but also effectively captured the differences in vug development patterns between different reservoir bodies, thus optimizing the simulation of the entire reservoir vug distribution. Ultimately, based on the incorporation of vug size distribution data, we successfully derived a more refined and accurate reservoir vug distribution model, as shown in Figure 1.

Table 3. The physical properties of cave dimensions in different regions of the target reservoir.

Unit	Associated Fracture–Vug System	Average Permeability/(mD)	Average Porosity/(%)	The Standard Deviation of Porosity in This Region and the Overall Porosity of the Reservoir/(%)	Reservoir Rock Type
AD22 Unit	AD22 Well Cluster	1526.38	17.93	3.325	carbonate rock
	TH12208 Well Cluster	1824.74	15.84	1.235	carbonate rock
	TH12201 Well Cluster	1833.09	11.01	3.595	carbonate rock
	TH12332 Well Cluster	1806.17	13.64	0.965	carbonate rock

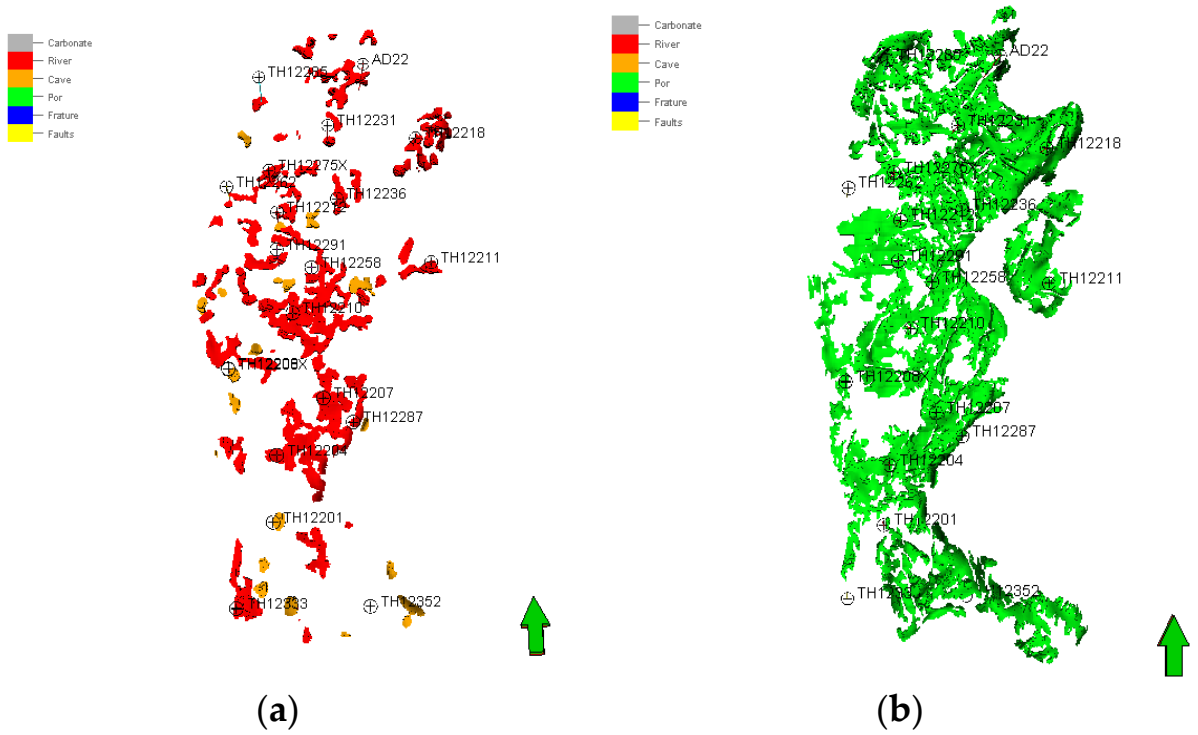


Figure 1. Numerical simulation framework model of the target reservoir ((**a**): framework model of vuggy reservoir body distribution; (**b**): reservoir vug distribution model). The arrow indicates the direction north.

Subsequently, based on existing geological exploration data, a fracture distribution model for the target reservoir was developed by incorporating reservoir fracture distribution parameters. This model was then integrated with the aforementioned reservoir vug distribution model to construct a comprehensive vug–fracture reservoir model. This high-precision model effectively characterizes the rock matrix framework of the reservoir, as shown in Figure 2.

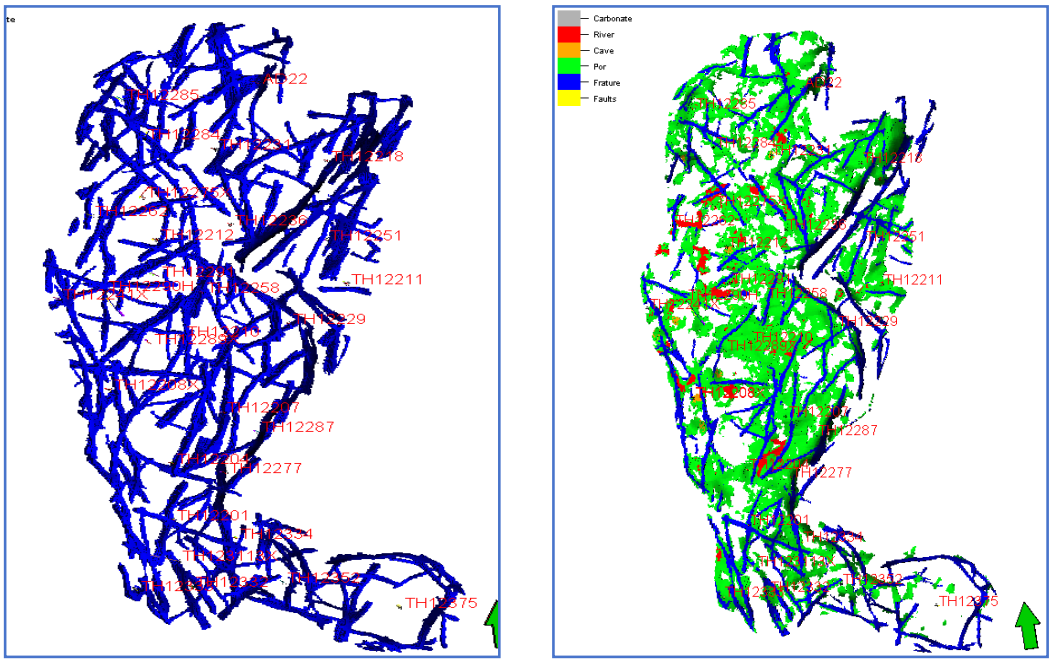


Figure 2. Comprehensive vug–fracture reservoir model of the target reservoir ((**a**): reservoir fracture model; (**b**): comprehensive reservoir vug–fracture model). The arrow indicates the direction north.

Based on the comprehensive vug–fracture reservoir model, the porosity parameters of different reservoir units were further incorporated. This process refined the assignment of porosity parameters through dynamic constraints and stratified calibration, thereby improving the accuracy of porosity predictions. During the inversion process, in order to accurately address discrepancies between high-porosity zones in the vuggy reservoir bodies and dynamic data, isolated single wells and connected well clusters were selected as inversion benchmarks to ensure the reliability and accuracy of the inversion results. Figure 3 shows the relationship between impedance inversion and porosity as well as porosity types. On the horizontal axis of Figure 3, the magnitude of the impedance inversion parameter is directly proportional to the effective space available for storing oil in the porosity. Lower impedance indicates larger fluid space in the pores, thus allowing for more effective space for oil storage. Specifically, impedance inversion helps to identify the porosity and porosity types in different regions of the reservoir. The vertical axis reflects the variation in different porosity regions, showing the transition from low-porosity to high-porosity areas. This relationship between impedance and porosity is achieved through an inversion model built on data from different well clusters and individual wells. The porosity systems of each well cluster are further classified into unfilled cavities, filled cavities, and other types of pore–fracture systems, which aids in identifying trends in the porosity variation and spatial distribution of porosity types in the reservoir. Therefore, Figure 3 not only illustrates the porosity distribution characteristics of different regions in the target block, but also lays the foundation for subsequent porosity parameter inversion and detailed characterization of porosity types within individual regions. This process provides effective support for further analysis of the reservoir, enabling more precise capture of porosity characteristics in different regions and offering a more detailed data foundation for reservoir development and management.

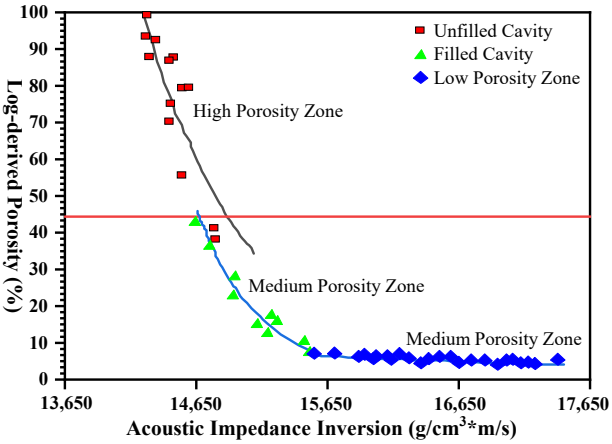


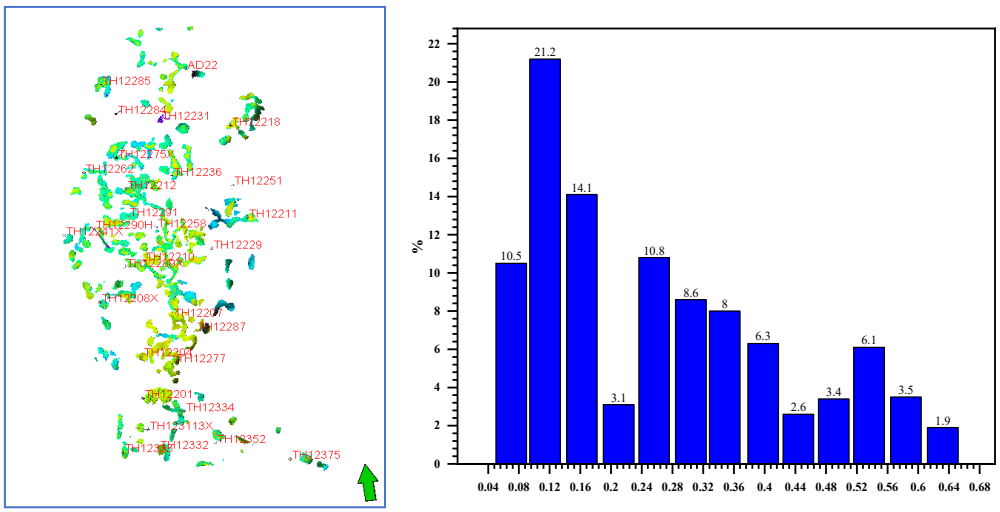
Figure 3. The relationship between wave impedance and porosity.

During dynamic inversion of vuggy porosity, parameter characterization was conducted based on reserve the calculation Formula (1):

$$\varphi = \frac{R \cdot B_o}{v \cdot s_o \cdot \rho} \quad (1)$$

Here, φ is the porosity, %; R is the dynamic reserve, m^3; B_o is the formation volume factor, m^3/m^3; v is the vug volume, m^3; s_o is the oil saturation, %; and ρ is the crude oil density, g/cm^3.

Through dynamic inversion of production data from well clusters in the target reservoir unit, an acoustic impedance versus vuggy porosity correlation was established, subsequently enabling the development of a vuggy porosity model. Inversion results demonstrate an average porosity of 23.7% in the target reservoir unit, with numerical values showing complete consistency with dissolution intensity variations observed in actual reservoir units, thereby validating the reliability of the dynamic inversion methodology, as shown in Figure 4.



(**a**) (**b**)

Figure 4. Porosity model of the target reservoir unit ((**a**): reservoir-wide porosity model structure; (**b**): reservoir-wide porosity distribution characteristics). The arrow indicates the direction north.

After completing the above work, further refinement of the model's porosity parameters was conducted. Based on the existing well log interpretation data, the reservoir model was divided into shallow and deep layers with a boundary at 160 m underground. Results

demonstrate that shallow vuggy porosity in the target reservoir unit significantly exceeds that of the mid–deep intervals, indicating more intensive karstification processes in shallow zones and revealing fracture-controlled porosity characteristics, as shown in Figure 5.

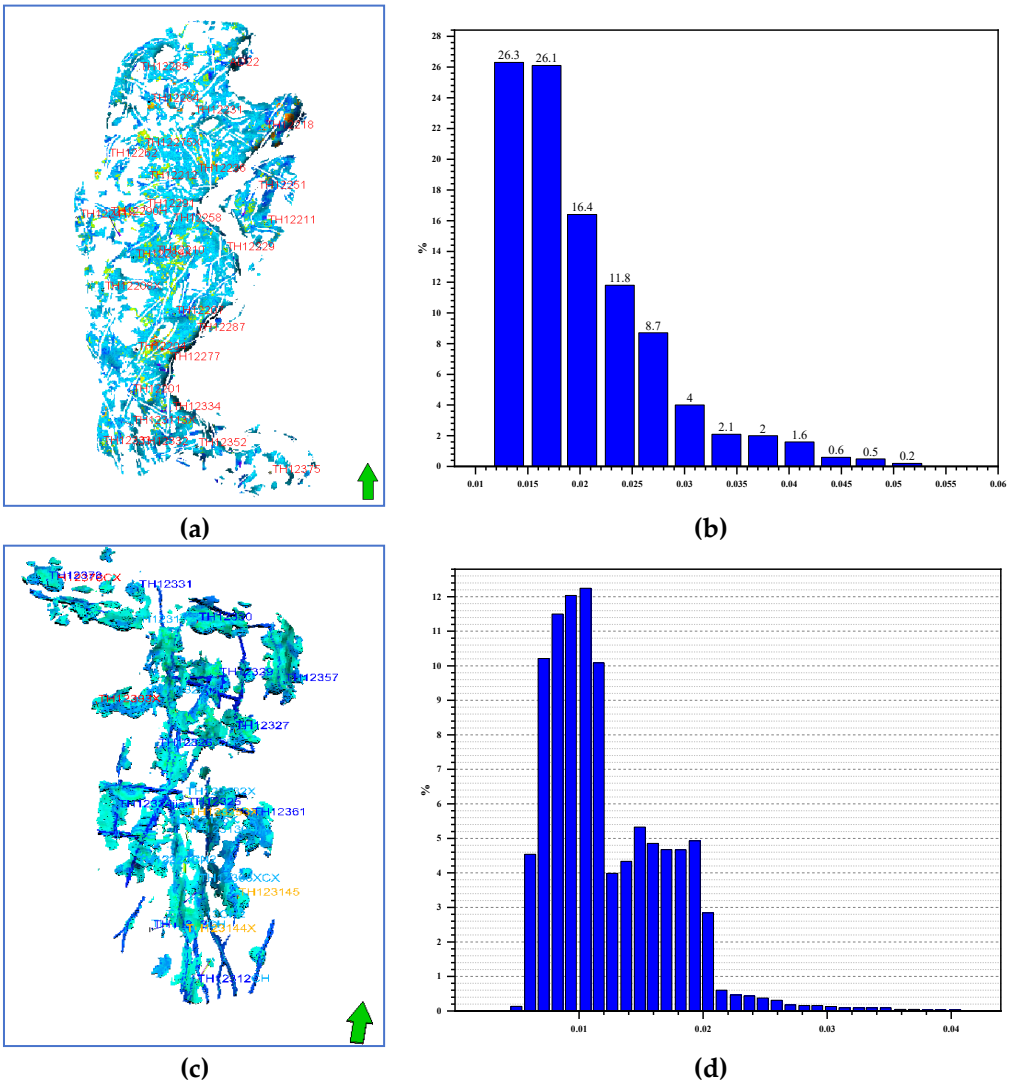


Figure 5. Porosity structure of shallow and deep zones in the target reservoir ((**a**): shallow zone porosity model structure; (**b**): shallow zone porosity distribution characteristics; (**c**): deep zone porosity model structure; (**d**): deep zone porosity distribution characteristics). The arrow indicates the direction north.

2.2. Reservoir Dynamic Reserve Characterization

The establishment of the target reservoir unit model in preceding chapters has defined the distribution characteristics of petrophysical parameters and pore–fracture structures. Building upon this foundation, it is essential to incorporate reservoir oil reserves and fluid content parameters to formulate a comprehensive reservoir unit model. In the development of carbonate fracture–vuggy reservoirs, dynamic reserve evaluation constitutes the critical component for optimizing development strategies. As a representative karst-controlled reservoir unit with complex geological architecture and differentiated aquifer energy distribution, the target reservoir unit exhibits substantial discrepancies in evaluation results when using conventional methodologies. To address this, the present study proposes an integrated technical framework centered on the DPM, synergistically combining modified material balance methods with modern production decline analysis. This systematic ap-

proach evaluates the dynamic reserves of the target reservoir unit while elucidating the influence mechanisms of strong, moderate, and weak aquifer energy on reserve drainage processes. In this section, we will explicitly discuss the assumptions underpinning the DPM, their potential impacts on results, and the sensitivity analysis of key parameters.

The DPM is based on several key assumptions: (1) Pseudo-Steady-State Flow Conditions: The model assumes that reservoir conditions are at a pseudo-steady state, meaning that the reservoir has reached a state in which pressure changes occur gradually, and flow rates remain relatively constant over time. This assumption simplifies the complex transient flow conditions typically encountered in oil reservoirs. (2) Uniform Aquifer Support: The model assumes that the aquifer surrounding the oil reservoir provides a consistent and uniform support across the entire reservoir. This assumption allows for simplified calculations and accurate reserve estimates under certain conditions but may lead to errors in the case of significant aquifer heterogeneity. (3) Constant Compressibility Factors: The compressibility factors for oil, water, and rock are assumed to remain constant throughout the reservoir's life cycle. While this assumption is generally valid for short-term predictions, it may introduce discrepancies in long-term dynamic reserve estimations, especially when dealing with large pressure variations; (4) Constant Flow Regimes: The model assumes that flow regimes remain consistent throughout the reservoir's development. This means that fluid flow is assumed to transition from pipe flow to seepage flow in a predictable manner, which can simplify the complex interactions that may arise in fractured–vuggy reservoirs with significant heterogeneity. These assumptions are critical to the functioning of the DPM. While they help simplify the model, their potential impact on results must be considered, especially in reservoirs exhibiting strong heterogeneity or undergoing extreme pressure changes.

Initially, the compressibility factor is defined as a function of formation pressure. Through integration from initial to current pressure conditions, the elastic drive material balance equation is re-derived as shown in Equation (2):

$$N_p B_o = N B_{oi} \left[\left(e^{-\int_{p_i}^{p} c_o dp} - 1 \right) + \frac{1}{S_{oi}} \left(1 - e^{\int_{p_i}^{p} c_p dp} \right) + \frac{S_{wi}}{S_{oi}} \left(e^{-\int_{p_i}^{p} c_w dp} - 1 \right) \right] \quad (2)$$

where N_p is the cumulative oil production, m^3; B_o is the formation volume factor, m^3/m^3; N is the original oil in place, m^3; B_{oi} is the initial formation volume factor, m^3/m^3; S_{oi} is the initial oil saturation, %; S_{wi} is the initial water saturation, %; p is the current pressure, Pa; p_i is the initial pressure, Pa; c_o is the oil compressibility, Pa^{-1}; c_p is the porosity compressibility, Pa^{-1}; and c_w is the water compressibility, Pa^{-1}.

Modern production decline analysis, grounded in the pseudo-steady-state flow characteristics of closed reservoirs, calculates dynamic reserves through the Blasingame-type curve matching of production data. This methodology proves particularly applicable to wells exhibiting extended flowing periods and comprehensive pressure monitoring data. However, its inherent limitations include inadequate sensitivity to aquifer size, liquid production rate fluctuations, and oil–water two-phase flow dynamics. In reservoirs with strong aquifer support, variations in aquifer multiples can induce substantial errors in dynamic reserve characterization accuracy. To overcome these constraints, this study advances the DPM, which differentiates conventional material balance equations to enable the precise identification of water invasion onset timing through staged pressure change analysis, while introducing a water invasion index to quantitatively characterize aquifer energy. Within this technical framework, accurate dynamic reserve estimation constitutes the cornerstone of oil drainage pathway analysis. Given the favorable interwell connectivity, pronounced well interference effects, and substantial aquifer energy observed in the target

reservoir unit, the proposed dynamic reserve methodology demonstrates applicability and yields reliable results.

First, aquifer-, oil body-, and well-related parameters are calculated. This calculation employs the material balance equations (Equations (3) and (4)), which require rigorous consideration of water–oil volume conservation:

$$NB_{oi}C_o(p_i - p_R) = N_pB_o + W_pB_w - W_e \tag{3}$$

where p_R is the reservoir pressure, Pa; W_p is the cumulative water production, m^3; B_w is the formation water volume factor, m^3/m^3; and W_e is the water injection volume, m^3.

$$W_e = N_wC_w(p_i - p_{aq}) \tag{4}$$

where N_w is the water volume, m^3; C_w is the water compressibility, Pa^{-1}; and p_{aq} is the aquifer pressure, Pa.

A modified term incorporating pseudo-steady-state water invasion conditions is introduced, accounting for the aquifer–oil body pressure differential as shown in Equation (5):

$$\frac{dW_e}{dt} = k(p_{aq} - p_R) \tag{5}$$

where t is time, s; k is the transmissibility coefficient, $m^3/(Pa{\cdot}s)$.

Additionally, a productivity equation is introduced, which accounts for the oil body–bottomhole pressure differential as shown in Equation (6):

$$q_L = \frac{d(N_pB_o + W_pB_w)}{dt} = J(p_R - p_{wf}) \tag{6}$$

where q_L is the production rate (m^3/s); J is the equilibrium index, $m^3/(Pa{\cdot}s)$; and p_{wf} is the bottomhole flowing pressure, Pa.

Subsequently, reservoir pressure parameters are calculated across discrete time steps, with each step corresponding to a system of three-variable linear equations. The pressure solution for each subsequent time step is iteratively derived from the preceding step, continuing until the predetermined simulation timeframe is reached. Detailed governing equations for this stepwise calculation are provided in Equations (7)–(11):

$$\frac{dp_R}{dt} + \frac{q_L}{n} - \frac{k}{n}(p_{aq} - p_R) = 0 \tag{7}$$

where n is the reservoir compaction parameter, m^3.

$$\frac{dp_{aq}}{dt} + \frac{k}{m}(p_{aq} - p_R) = 0 \tag{8}$$

where m is the water volume compaction parameter, m^3.

$$q_L = J(p_R - p_{wf}) \tag{9}$$

$$m = N_wC_w \tag{10}$$

$$n = NB_{oi}C_o \tag{11}$$

In the above calculation process, the prior introduction of initial conditions is required, as specified in Equations (12) and (13):

$$t = 0 \tag{12}$$

$$p_{aq} = p_r = p_{wf} = p_t \tag{13}$$

where p_t is the equilibrium pressure, Pa.

Initial boundary conditions are provided in Equations (14) and (15):

$$t > 0 \tag{14}$$

$$q_L = q_t \tag{15}$$

where q_t is the total production rate (m^3/s).

In the aforementioned parameters, the total production rate q_t is positive during well production and negative during injection operations. Subsequently, by adjusting parameters k and J and the water–oil volumes, the cumulative liquid production–bottomhole flowing pressure curve is history matched. The pressure parameter expressions governing this process are provided in Equations (16) to (18):

$$p_{Rt} - p_{Rt-1} + \frac{kdt}{n}(p_{aqt} - p_{Rt}) = 0 \tag{16}$$

$$p_{aqt} - p_{aqt-1} + \frac{kdt}{m}(p_{aqt} - p_{Rt}) = 0 \tag{17}$$

$$q_L = J(p_{Rt} - p_{wft}) \tag{18}$$

where p_{Rt} and $p_{Rt\text{-}1}$ are the reservoir pressure at the current and previous time steps, Pa; p_{aqt} and $p_{aqt\text{-}1}$ are the aquifer pressure at the current and previous time steps, Pa.

The matrix form is shown in Equation (19):

$$\begin{bmatrix} -\frac{kdt}{n} & \frac{kdt}{n}+1 & 0 \\ \frac{kdt}{m}+1 & -\frac{kdt}{m} & 0 \\ 0 & J & -J \end{bmatrix} \begin{bmatrix} p_{aqt} \\ p_{Rt} \\ p_{wft} \end{bmatrix} = \begin{bmatrix} p_{Rt-1} - \frac{q_L dt}{n} \\ p_{aqt-1} \\ q_L \end{bmatrix} \tag{19}$$

where P_{wft} is the bottomhole flowing pressure at various time steps, Pa.

This methodology extends reservoir characterization parameters from conventional porosity and permeability to karst-specific features, including fracture–vug structures, vug volumes, and fracture conductivity. It further differentiates flow regimes into pipe flow, seepage flow, and coupled flow interactions, achieving superior accuracy compared to conventional approaches. Building upon this framework, dynamic reserve characterization of the target reservoir unit is completed, with these parameters integrated into the previously established reservoir model. The final numerical model enables precise history matching of production data and comprehensive evaluation of development strategies.

To further enhance the credibility of the DPM and ensure that the model can accommodate variations in real-world conditions, a sensitivity analysis of key parameters was conducted. This analysis explores how changes in aquifer properties, reservoir pressure, and fluid compressibility impact the accuracy of dynamic reserve calculations. (1) Aquifer Energy: The sensitivity of the model to variations in aquifer energy was assessed by adjusting the aquifer pressure and transmissibility coefficient in the model. This analysis showed that the model's reserve estimates are highly sensitive to the aquifer's transmissibility. In reservoirs with strong aquifer support, small variations in aquifer properties can lead to substantial changes in dynamic reserve estimates. Conversely, in reservoirs with weak aquifer support, the model's results are less sensitive to these parameters, but caution is still necessary when interpreting the results. (2) Oil–Water Two-Phase Flow Dynamics: Given that the target reservoir contains both oil and water, the sensitivity of the model to two-phase flow dynamics was analyzed. It was found that the liquid production rate

fluctuations and oil–water relative permeability can significantly affect the accuracy of the reserve calculations, especially in reservoirs with complex fluid flow regimes. In such cases, a more refined model that accounts for capillary pressure and relative permeability variations may be necessary. (3) Pressure Transients: The model's response to variations in reservoir pressure was tested by simulating different pressure decline scenarios. The analysis revealed that the model is highly sensitive to initial pressure conditions, especially in reservoirs with large initial pressure gradients. Accurate pressure monitoring and early-stage data are critical for obtaining reliable reserve estimates. The sensitivity analysis results underscore the importance of considering reservoir-specific characteristics when applying the DPM. While the method provides reliable estimates under certain conditions, adjustments to the model parameters may be necessary to improve accuracy in more complex reservoirs.

3. Results and Analysis

3.1. Reservoir Dynamic Reserve Characterization and Development Effectiveness Evaluation

Based on the aforementioned model and reservoir dynamic reserve characterization methodology, the total geological reserves of the target reservoir unit are determined to be 30.495 million metric tons. Analysis reveals that 53.7% of these reserves are concentrated within subterranean river reservoir bodies, with an additional 60.4% located in shallow intensely karstified zones at depths shallower than 160 m below surface. Detailed reserve distributions are tabulated in Table 4, with corresponding geological visualization provided in Figure 6.

Table 4. Reserve calculation summary of the target unit.

	Unit	Carved Body Volume 10^4 m^3	Porosity Volume 10^4 m^3	Geological Reserves (10^4 t)	Percentage (%)
	Total	158,347	4069	3049.5	
By Type	Subterranean River	7270	2187	1633.07	53.74
	Fault-controlled Cavities	2012	610	454.80	14.97
	Superficial Pores	42,887	705	526.77	17.34
	Deep Pores	55,861	1013	230.28	7.58
	Fractures	93,204	259	192.86	6.35
By Depth	0–160 m	91,087	2457	1834.56	60.37
	160 m—Oil Column Base	67,260	1612	1204.17	39.63

Through compartmentalized reservoir body modeling, dynamically constrained porosity inversion, and priority-based data fusion, this study systematically reveals the karst-controlled reservoir mechanisms and reserve distribution characteristics of the target reservoir unit. The modeling results demonstrate that subterranean river conduits and fault-controlled composite reservoir bodies constitute the primary hydrocarbon accumulations, exhibiting substantial reserve volumes with shallow zone enrichment. Overall, the target unit has a depth of approximately 325 m. When divided into shallow and deep layers with a boundary at 160 m underground, over 60% of the recoverable reserves are concentrated in the shallow layer, while the remaining 40% are located in the deep layer. Additionally, most of these recoverable crude oil reserves are concentrated in the dark rivers and various cave structures within the reservoir. These findings establish a scientific foundation for formulating development strategies and provide technical references for

analogous reservoir modeling and development planning. Based on the established model, the production performance of individual wells within the block was evaluated, determining the developable dynamic reserves of the target reservoir unit as 25.94 million metric tons. By inputting historical development parameters aligned with current operational practices, the model-derived current crude oil production closely matches field data with an overall error margin of 2.04%, confirming the numerical model's reliability. Further analysis indicates a current recovery factor of merely 12.6% for this reservoir unit, with detailed results presented in Figure 7.

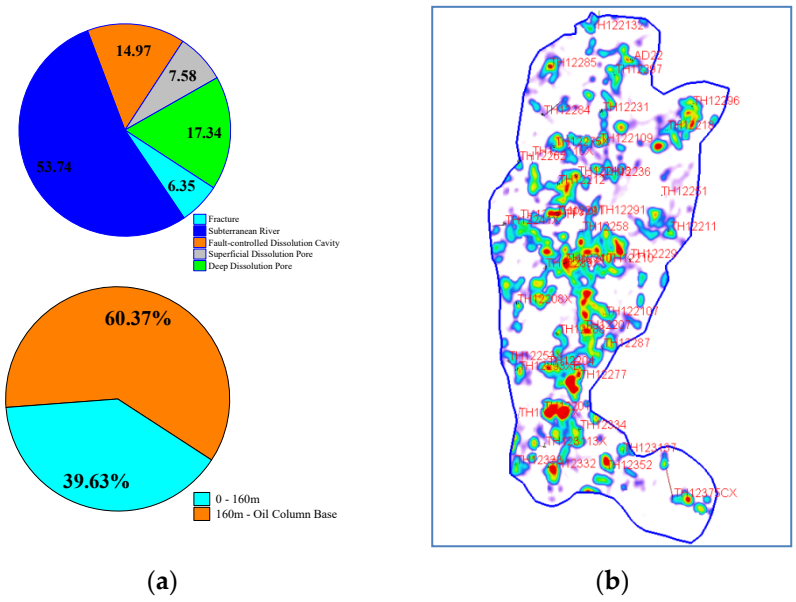


Figure 6. Modeling results of the target reservoir unit ((**a**): reserve distribution of the target reservoir unit; (**b**): hydrocarbon abundance map of the target reservoir unit).

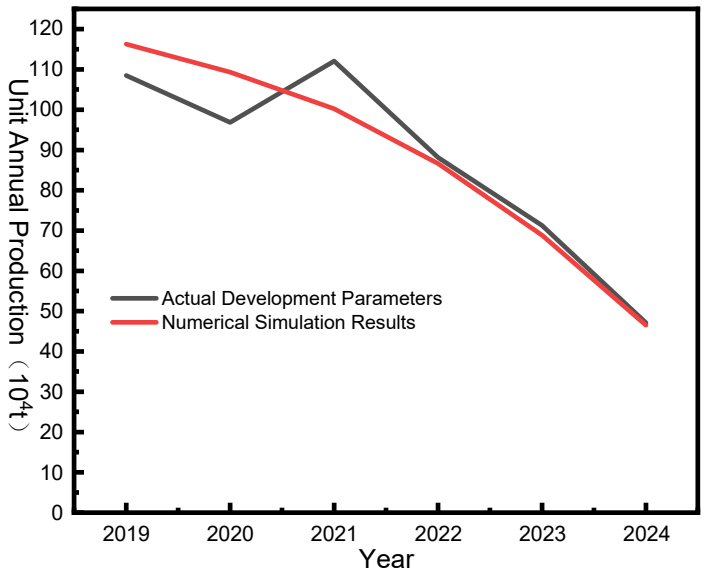
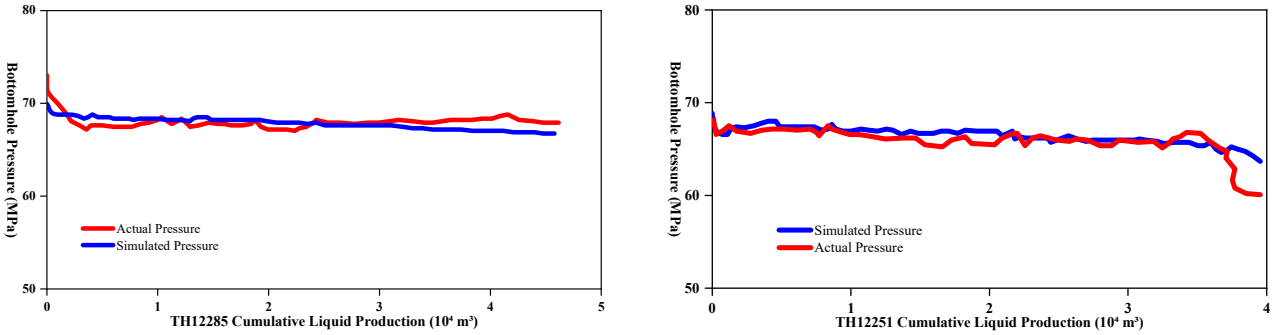


Figure 7. Comparison of numerical simulation history-matching parameters and actual development parameters for the target reservoir unit.

In addition to the above content, the model results show that the reserve utilization at different production wells with varying bottom water energy in the target reservoir unit exhibits significant differences. Specifically, well clusters with strong aquifer energy exhibit

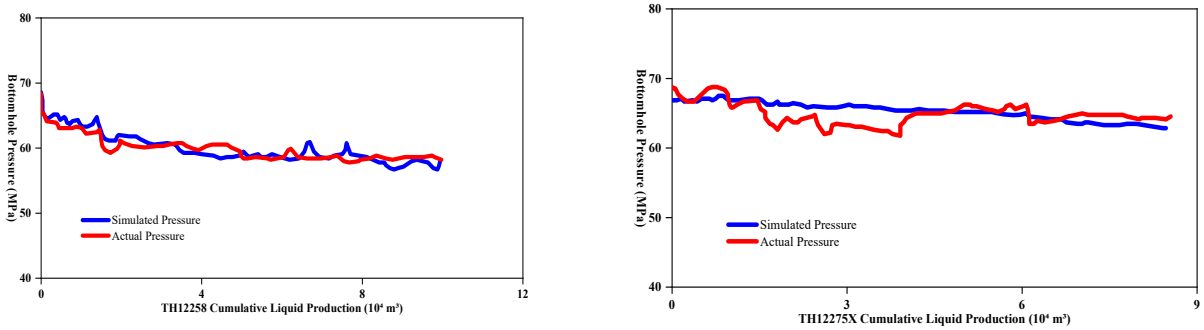
an average aquifer multiple of 17 and an aquifer energy index of 8 $m^3/(MPa \cdot d)$. These wells demonstrate universally low dynamic reserve recovery factors (<10%), attributable to rapid near-well reserve depletion caused by high water invasion rates. This process drives the migration and entrapment of undrained oil into distal subterranean river conduits. Compared to the strong bottom water energy zone, the wells in the medium bottom water energy zone will not lead to a rapid breakthrough of bottom water, thus maintaining a better distribution of oil, gas, and water. Water injection can help maintain a more stable development process and push oil and gas towards production wells. In this case, the water injection efficiency is higher, and in the medium bottom water energy zone, water can be injected more uniformly, avoiding the rapid breakthrough of bottom water, which is more effective than in the strong bottom water energy zone. The reservoir development status in the medium bottom water energy zone is shown in Figure 8.



(**a**) (**b**)

Figure 8. Case studies of well-controlled reserve calculation for strong aquifer energy wells in the target reservoir unit ((**a**): Case 1; (**b**): Case 2).

In contrast to well clusters with strong aquifer energy, those exhibiting moderate aquifer energy (aquifer multiple: 5–10 times) demonstrate more significant improvements in waterflood displacement efficiency. However, the water blocking effect induced by fracture fillings substantially constrains the drainage efficiency of distal reserves in these areas, as exemplified in selected cases shown in Figure 9.

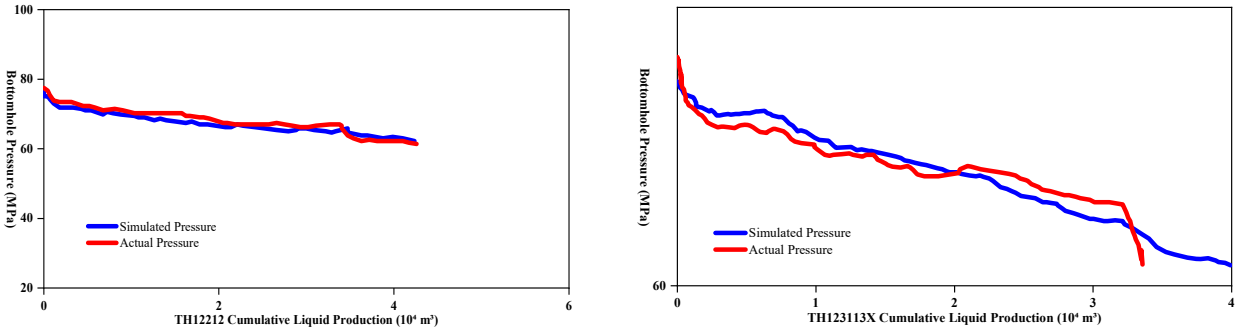


(**a**) (**b**)

Figure 9. Case studies of well-controlled reserve calculation for moderate aquifer energy wells in the target reservoir unit ((**a**): Case 1; (**b**): Case 2).

In addition to the aforementioned well clusters, the target reservoir unit contains clusters with weak aquifer energy (aquifer multiple < 3 times). The oil drainage process in these wells is primarily driven by in situ elastic energy, achieving an overall dynamic reserve drainage efficiency exceeding 90%. The remaining potential is concentrated in unswept vuggy zones, as illustrated in Figure 10. In the weak bottom water energy zone, due

to insufficient bottom water driving force, the bottom water cannot rapidly break through to the production wells, resulting in a more uniform distribution of oil and gas. This uniform distribution of oil and gas provides a longer time window for reservoir extraction, reducing the impact of water invasion on oil and gas during the development process, thereby enhancing the development potential of the area. Generally, the development in the weak bottom water zone is relatively stable, with oil and gas extraction and water injection progressing gradually. This can avoid the negative effects of early water invasion and improve the recovery rate of oil and gas. Since the bottom water driving force is weak, water injection and other auxiliary development methods need to operate over a longer development cycle.



(**a**) (**b**)

Figure 10. Case studies of well-controlled reserve calculation for weak aquifer energy wells in the target reservoir unit ((**a**): Case 1; (**b**): Case 2).

From the well cluster perspective, the target reservoir unit exhibits an estimated reserve drainage efficiency of 90.6%. However, the current crude oil recovery factor derived from history-matched data and field development parameters remains approximately 10% of the drainable reserves. This discrepancy primarily stems from significant aquifer energy variations caused by major fault zones. Specifically, fault intersection zones demonstrate active aquifer energy, whereas peripheral zones suffer from energy attenuation, leading to substantial differences in oil displacement energy across well clusters. The resulting disparities in recovery factors are quantitatively detailed in Table 5.

Table 5. Reserve drainage status and current recovery factor of different well clusters in the target reservoir unit.

Unit	Associated Fracture-Vug System	Well Count	Static Reserves 10^4 t	Dynamic Reserves 10^4 t	Production 10^4 t	Drainage Efficiency %	Recovery Factor %
AD22Unit	AD22 Well Cluster	14	943	873.5	108.3	92.6	11.5
	TH12208 Well Cluster	10	910.5	824.5	113	90.6	12.4
	TH12201 Well Cluster	7	685	635	67.9	92.7	9.9
	TH12332 Well Cluster	12	511	261	36.7	51.1	7.2
	Subtotal	43	3049.5	2594	325.9	85.1	10.7

3.2. Discussion on Development Strategies Based on Reservoir Aquifer Energy Classification

When designing development plans tailored to reservoir characteristics, it is imperative to comprehensively account for reservoir heterogeneity, particularly the spatial variability of aquifer energy under the dual influences of fault properties and karst intensity. Research demonstrates that aquifer energy intensity correlates closely with structural features, rock permeability, and aquifer distribution. Specifically, the NE-trending main faults and their intersections in the target reservoir unit, characterized by superior fracture conductivity, serve as primary pathways for rapid aquifer propagation along fault

planes. These zones typically exhibit strong aquifer energy with water coning rates exceeding 15 times aquifer multiples, forming efficient water drive systems that result in low oil–water displacement efficiency. Consequently, the development of these areas necessitates early implementation of enhanced oil recovery techniques such as gas injection or nano-fluid imbibition to mitigate water channeling and delay adverse waterflood impacts.

In contrast, other regions of the unit contain weathering crust karst zones dominated by vug-fracture networks, exhibiting moderate aquifer energy levels with uniform aquifer advancement patterns. In these areas, aquifer propagation occurs gradually through high-permeability conduits (e.g., fractures and vugs), typically showing aquifer multiples between 5 and 10. Development strategies here should prioritize optimizing water injection timing and intensity. This involves dynamically adjusting injection–production parameters and rationally utilizing fracture connectivity indices to ensure steady aquifer advancement while preventing premature water breakthrough. For zones influenced by secondary faults or isolated fault–karst bodies, poor fracture/vug connectivity results in weak aquifer energy (aquifer multiples < 3). These low-energy regions require precision energy-enhancement measures. Targeted hydraulic fracturing can effectively activate distal vug reserves, improving hydrocarbon productivity. Concurrently, water injection stimulation technologies may be deployed to optimize waterflood efficiency, ensuring effective fluid displacement and enhanced recovery.

The aforementioned dynamic reserve evaluation based on numerical modeling provides a scientific foundation for implementing these strategies. Analysis of reservoirs with different aquifer energy levels indicates that strong bottom water energy zones typically have a higher bottom water driving force, allowing bottom water to quickly break through to the production wells, leading to serious water invasion issues and reduced oil–water displacement efficiency. In such cases, conventional waterflooding techniques may not effectively control water invasion, limiting the oil and gas recovery rate. To reduce water channeling phenomena and improve recovery efficiency, early gas injection or nano-fluid imbibition techniques must be employed. Gas injection (such as CO_2 or nitrogen) can reduce the rate at which bottom water invades the oil layer, and through the "gas cap effect" of the injected gas, it can form pressure support within the reservoir, pushing oil and gas toward the production wells. The low density and flow characteristics of gas allow it to effectively replace water as the driving force, reducing the impact of water invasion. In this study, the use of CO_2 injection was considered to optimize the regional development performance. The results show that the recovery rate in a certain area increased with the rise in CO_2 injection pressure. As the injection pressure increased from 8 MPa to 16 MPa, the recovery rate in the local area rose from 43.24% to 66.71%. This indicates that CO_2 effectively inhibited water invasion and supplemented the oil displacement energy in the formation. However, for every 2 MPa increase in pressure, the rate of recovery increase dropped by 62.21%, and the reservoir permeability gradually decreased by 3.89%. It is speculated that the pressure increase promoted CO_2-induced asphaltene precipitation within the crude oil, which inhibited the flow of crude oil in both the reservoir and the wellbore, reducing the extent of recovery rate increase [19,27]. Nevertheless, overall, this development method remains a feasible system for optimizing crude oil recovery benefits. Nano-fluids, on the other hand, can improve the wettability of the oil–water interface, reduce interfacial tension, and enhance the drive efficiency of oil and gas. The injection of nano-fluids can effectively improve the displacement efficiency of oil and gas, reducing the interference of water invasion on production. By applying these technologies, it is possible to effectively reduce water invasion in strong bottom water energy zones, increase oil and gas recovery rates, and optimize the production structure of oil and gas.

In reservoirs with moderate bottom water energy, the bottom water driving force is moderate, and water injection can effectively promote the flow of oil and gas. However, the rate of water invasion is relatively slow, so the timing, intensity, and distribution of water injection are crucial. If water injection is conducted too early or too quickly, it may lead to the early breakthrough of bottom water and cause uneven water invasion. Conversely, if water injection is delayed, it may fail to effectively maintain reservoir pressure, impacting recovery rates. Therefore, in these zones, optimizing the timing and intensity of water injection is essential to ensure uniform water advancement and avoid issues such as excessive or untimely water injection. By dynamically adjusting the water injection intensity based on reservoir pressure and oil and gas distribution, reservoir pressure can be effectively maintained, and oil and gas recovery can be improved. In moderate bottom water energy reservoirs, the connectivity of fractures plays an important role in oil and gas recovery. By dynamically adjusting fracture connectivity, the waterflooding efficiency can be optimized, avoiding excessive closure or opening of fractures, which in turn enhances oil and gas flow efficiency. These strategies ensure that, while maintaining appropriate water injection intensity, oil and gas distribution remains uniform, reducing the impact of water invasion and improving oil and gas recovery. Additionally, the development approach can be flexibly adjusted based on the actual conditions of the reservoir to achieve optimal development outcomes.

In the weak bottom water energy zone, the driving force of bottom water is relatively weak, and the natural flow of oil and gas is slow, making it difficult to mobilize distal reserves and resulting in low recovery rates. Relying solely on bottom water drive is not effective for developing the entire reservoir. Therefore, it is essential to enhance oil and gas mobility through techniques such as hydraulic fracturing and water injection stimulation, particularly to activate distal reserves. Hydraulic fracturing technology can significantly increase the fracture permeability of the reservoir, creating more flow pathways. In weak bottom water zones, the formation and expansion of fractures can greatly improve the mobility and recovery rate of oil and gas. After fracturing, the effective porosity and permeability of the reservoir increase, providing more space for oil and gas extraction. Additionally, water injection stimulation technology can artificially inject water to maintain or enhance reservoir pressure, facilitating oil and gas flow. Water injection can effectively activate distal reserves in weak bottom water zones, improving oil and gas recovery efficiency. By combining hydraulic fracturing and water injection stimulation, not only can the mobility of oil and gas be enhanced, reducing water invasion and improving recovery rates, but distal reserves can also be activated, further boosting development benefits. These technologies are especially important in weak bottom water areas, as these zones lack sufficient bottom water energy to support oil and gas extraction.

The differentiated development strategies for these three reservoir zones are tailored to the characteristics of their respective bottom water energy levels, using targeted technical approaches to maximize oil and gas recovery. These strategies can effectively address the development challenges posed by different bottom water energy zones and improve the overall reservoir development efficiency. As demonstrated in Figure 11, the application of these differentiated reserve utilization strategies has achieved significant crude oil production increases in the target reservoir unit. The model output data prediction indicates that this strategy can achieve an overall secondary increase in oil production from the reservoir over the next three years, with an 81.66% improvement compared to the previous years' baseline. Ultimately, the increase in the comprehensive recovery rate will further rise by 10.7%. This successful case establishes a scientific framework for the efficient development of ultra-deep karst reservoirs and provides actionable experience and paradigms for analogous reservoirs.

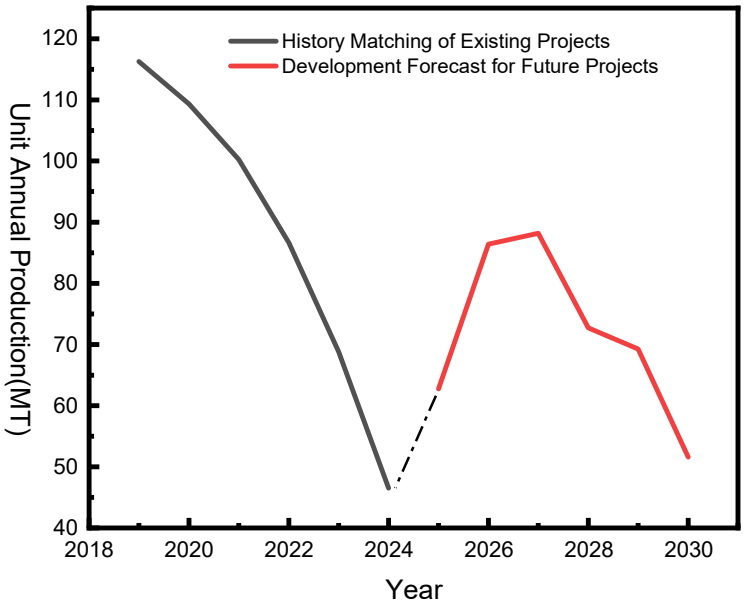


Figure 11. Prediction and historical matching results of development performance parameters for the optimized target reservoir unit.

4. Conclusions

This study, focusing on the target reservoir unit, systematically reveals the karst-controlled reservoir mechanisms and reserve distribution characteristics through compartmentalized reservoir body modeling, dynamically constrained porosity inversion, and priority-based data fusion. The unit's core reservoirs are dominated by subterranean river conduits and fault-controlled composite bodies, exhibiting substantial reserve volumes with shallow zone enrichment, where conventional development methods proved inadequate for efficient reserve extraction. Based on these findings, differentiated development strategies were formulated for two distinct reservoir units, providing critical technical references for analogous karst reservoir modeling and development. Furthermore, dynamic reserve evaluation using the Differential Processing Method integrated with numerical simulations demonstrates that innovative geological-dynamic integration successfully uncovers the heterogeneity of reserve utilization and aquifer energy classification mechanisms in ultra-deep karst reservoirs. In strong aquifer energy zones, reserve extraction is governed by dual controls of fault–karst coupling, where rapid water coning induces significant water invasion inhibitory effects, compromising oil–water displacement efficiency. Moderate energy zones exhibit substantial synergistic potential in injection-production operations; dynamic adjustment of operational parameters can markedly enhance recovery efficiency. Conversely, weak energy zones require artificial interventions such as hydraulic fracturing and water injection stimulation to activate distal reserves and unlock their potential. This research establishes a scientific quantitative basis for targeted, differentiated development strategies across aquifer energy zones and lays a methodological foundation for the dynamic evaluation and development optimization in analogous reservoirs. By assessing critical parameters such as aquifer energy through numerical modeling and implementing regionalized differentiated strategies, the study significantly improves reservoir development efficiency, demonstrating profound academic value and practical significance.

Author Contributions: Methodology, H.S., F.Y. and C.Z.; Software, S.Z., F.Y., L.L. and Y.F.; Investigation, H.S. and C.Y.; Data curation, H.S., S.Z., L.L. and Y.F.; Writing—original draft, H.S. and C.Y.; Writing—review & editing, C.Z.; Supervision, C.Z. All authors have read and agreed to the published version of the manuscript.

Funding: This research was funded by the National Science and Technology Major Project of China (2016ZX05053) and the Science and Technology Department Project of Sinopec-China petroleum (P11089).

Data Availability Statement: The original contributions presented in this study are included in the articles. Further inquiries can be directed to the corresponding author(s).

Acknowledgments: We are grateful to the Shandong Engineering Research Center for CO_2 Utilization and Storage for their kind help in this study. The valuable comments made by the anonymous reviewers are also sincerely appreciated.

Conflicts of Interest: Authors: Hongwei Song, Shiliang Zhang, Feiyu Yuan, Lu Li, Yafei Fu, and Chao Yu are employed by the Sinopec Northwest Oilfield Company. The authors declare that the research was conducted in the absence of any commercial or financial relationships that could be construed as a potential conflict of interest.

References

1. Li, Y.; Kang, Z.; Xue, Z.; Zheng, S. Theories and practices of carbonate reservoirs development in China. *Pet. Explor. Dev.* **2018**, *45*, 712–722. [CrossRef]
2. Tang, B.; Ren, K.; Lu, H.; Li, C.; Geng, C.; Wei, L.; Chai, Z.; Wu, S. Study on residual oil distribution law during the depletion production and water flooding stages in the fault-karst carbonate reservoirs. *Processes* **2023**, *11*, 2147. [CrossRef]
3. Liu, P.; Jiang, L.; Tang, B.; Ren, K.; Huang, M.; Geng, C. Residual Oil Distribution Pattern in a Fault-Solution Carbonate Reservoir and Countermeasures to Improve Oil Development Effectiveness. *Geofluids* **2022**, *2022*, 2147200. [CrossRef]
4. Liu, Y.; Rui, Z.; Yang, T.; Birol, D. Using Propanol as an Additive to CO_2 for Improving CO_2 Utilization and Storage in Oil Reservoirs. *Appl. Energy* **2022**, *311*, 118640. [CrossRef]
5. Wang, J.; Zhao, W.; Liu, H.; Liu, F.; Zhang, T.; Dou, L.; Yang, X.; Li, B. Inter-well interferences and their influencing factors during water flooding in fractured-vuggy carbonate reservoirs. *Pet. Explor. Dev.* **2020**, *47*, 1062–1073. [CrossRef]
6. Tang, B.; Geng, C.; Huang, M.; Lu, H.; Ren, K. Research on the Depletion and Recovery Characteristics of Fault-Karst Reservoirs. *Geofluids* **2022**, *2022*, 1105335. [CrossRef]
7. Kouassi, A.K.F.; Pan, L.; Wang, X.; Wang, Z.; Mulashani, A.K.; James, F.; Shaame, M.; Hussain, A.; Hussain, H.; Nyakilla, E.E. Identification of karst cavities from 2D seismic wave impedance images based on Gradient-Boosting Decision Trees Algorithms (GBDT): Case of ordovician fracturevuggy carbonate reservoir, Tahe Oilfield, Tarim Basin, China. *Energies* **2023**, *16*, 643. [CrossRef]
8. Shi, W.; Cheng, J.; Liu, Y.; Gao, M.; Tao, L.; Bai, J.; Zhu, Q. Pressure transient analysis of horizontal wells in multibranched fault-karst carbonate reservoirs: Model and application in SHB oilfield. *Pet. Sci. Eng.* **2023**, *220*, 111167. [CrossRef]
9. Yue, P.; Xie, Z.; Huang, S.; Liu, H.; Liang, S.; Chen, X. The application of N2 huff and puff for IOR in fracture-vuggy carbonate reservoir. *Fuel* **2018**, *234*, 1507–1517. [CrossRef]
10. Qu, M.; Hou, J.; Qi, P.; Zhao, F.; Ma, S.; Churchwell, L.; Wang, Q.; Li, H.; Yang, T. Experimental study of fluid behaviors from water and nitrogen floods on a 3-D visual fractured-vuggy model. *J. Pet. Sci. Eng.* **2018**, *166*, 871–879. [CrossRef]
11. Cheng, H.; Yuan, F.; Zhang, S.; Li, L.; Luo, X.; Chen, B. Investigation on Water Invasion Mode and Remaining Oil Utilization Rules of Fractured-Vuggy Reservoirs: A Case Study of the Intersection Region of S99 Unit in Tahe Oilfield. *J. Process.* **2023**, *11*, 1833. [CrossRef]
12. Sun, Q.; Zhang, N.; Fadlelmula, M.; Wang, Y. Structural regeneration of fracture-vug network in naturally fractured vuggy reservoirs. *J. Pet. Sci. Eng.* **2018**, *165*, 28–41. [CrossRef]
13. Jiao, F. Practice and knowledge of volumetric development of deep fractured-vuggy carbonate reservoirs in Tarim Basin, NW China. *Pet. Explor. Dev.* **2019**, *46*, 576–582. [CrossRef]
14. Wang, J.; Liu, H.; Ning, Z.; Zhang, H.; Hong, C. Experiments on water flooding in fractured-vuggy cells in fractured-vuggy reservoirs. *Pet. Explor. Dev.* **2014**, *41*, 74–81. [CrossRef]
15. Wang, J.; Liu, H.; Zhang, J.; Meng, Q.; Liu, H.; Ge, L.; Zhu, Z.; Liu, Z. Experimental investigation on water flooding and continued EOR techniques in buried-hill metamorphic fractured reservoirs. *J. Pet. Sci. Eng.* **2018**, *171*, 529–541. [CrossRef]
16. Yue, P.; Xie, Z.; Liu, H.; Chen, X.; Guo, Z. Application of water injection curves for the dynamic analysis of fractured-vuggy carbonate reservoirs. *J. Pet. Sci. Eng.* **2018**, *169*, 220–229. [CrossRef]
17. Zheng, S.; Yang, M.; Kang, Z.; Liu, Z.; Long, X.; Liu, K.; Li, X.; Zhang, S. Controlling factors of remaining oil distribution after water flooding and enhanced oil recovery methods for fracture-cavity carbonate reservoirs in Tahe Oilfield. *Pet. Explor. Dev.* **2019**, *46*, 786–795. [CrossRef]
18. Xiao, Y.; Zhang, Z.; Jiang, T.; Cai, Z.; Deng, X.; Zhou, J. Dynamic and static combination method for fracture-vug unit division of fractured-vuggy reservoirs. *Arab. J. Sci. Eng.* **2018**, *43*, 2633–2640. [CrossRef]

19. Yang, M.; Li, X.; Tan, T.; Li, Q.; Liu, H.; Zhang, Y. Remaining oil distribution and potential tapping measures for palaeo-subterranean river reservoirs: A case study of TK440 well area in Tahe Oilfield. *Reserv. Eval. Dev.* **2020**, *10*, 43–48.
20. Lv, Q.; Zheng, R.; Zhou, T.; Guo, X.; Wang, W.; Li, J.; Liu, Z. Visualization study of CO2-EOR in carbonate reservoirs using 2.5 D heterogeneous micromodels for CCUS. *Fuel* **2022**, *330*, 125533. [CrossRef]
21. Yang, Y.; Rong, G.; Xin, Y.; Song, Y.; Li, B. Visualization Experimental Investigation on Flow Regulation and Oil Displacement Characteristics of Gel Foam in Fractured-Vuggy Carbonate Reservoirs. *ACS Omega* **2024**, *9*, 40810–40820. [CrossRef]
22. Zhang, C.; Gu, Z.; Li, P.; Xu, G.; Zhang, D.; Li, Z. Investigation on the condensate gas composition variation and wax deposition mechanism during temperature-induced phase transition process. *J. Clean. Prod.* **2024**, *442*, 141109. [CrossRef]
23. Li, J.; Feng, Y.; Wang, J.; Xu, Z.; Li, B.; Zhang, C. Study on Formation and Migration Law of Foam in Fractures and Its Influencing Factors. *ACS Omega* **2024**, *9*, 24362–24371. [CrossRef]
24. Zhang, C.; Yu, C.; Gu, Z.; Liu, K.; Wu, P.; Li, Z. Characterization and optimization of oil-gas interfacial tension during CO_2/N_2 injection in heavy oil reservoirs: Experimental study and regression model. *Pet. Sci.* **2025**, *06*, 24. [CrossRef]
25. Hu, X.; Zheng, W.; Zhao, X.; Niu, B. Quantitative characterization of deep fault-karst carbonate reservoirs: A case study of the Yuejin block in the Tahe oilfield. *Energy Geosci.* **2023**, *4*, 100153. [CrossRef]
26. Azizollah, K.; Anar, R.; Dmitry, I. The control of asphaltene precipitation in oil wells. *Pet. Sci. Technol.* **2018**, *36*, 443–449.
27. Xu, Z.; Li, Z.; Cui, S.; Li, B.; Chen, D.; Zhang, Q.; Zheng, L.; Husein, M.M. Flow characteristics and EOR mechanism osf foam flooding in fractured vuggy reservoirs. *J. Pet. Sci. Eng.* **2022**, *211*, 110170. [CrossRef]
28. Tang, H.; Juan, H.; Rong, Y.; Li, X. Study on water drive law and characteristics of remaining oil distribution of typical fault-karst in faultkarst reservoirs, Tahe Oilfield. *Editor. Dep. Pet. Geol. Recovery Effic.* **2018**, *25*, 95–100.
29. Cao, L.; Sun, J.; Zhang, B.; Lu, N.; Xu, Y. Sensitivity analysis of the temperature profile changing law in the production string of a high-pressure high-temperature gas well considering the coupling relation among the gas flow friction, gas properties, temperature, and pressure. *Front. Phys.* **2022**, *10*, 1050229. [CrossRef]
30. Wei, C.; Cheng, S.; Chen, G.; Shi, W.; Wu, J.; Wang, Y.; Yu, H. Parameters evaluation of fault-karst carbonate reservoirs with vertical beads-on-string structure based on bottom-hole pressure: Case studies in Shunbei Oilfield, Tarim Basin of Northwestern China. *Oil Gas Sci. Technol.* **2021**, *76*, 59. [CrossRef]
31. Cao, L.; Sun, J.; Liu, J.; Liu, J. Experiment and Application of Wax Deposition in Dabei Deep Condensate Gas Wells with High Pressure. *Energies* **2022**, *15*, 6200. [CrossRef]
32. Cheng, H. The Enhanced Oil Recovery Effect of Nitrogen-Assisted Gravity Drainage in Karst Reservoirs with Different Genesis: A Case Study of the Tahe Oilfield. *Processes* **2023**, *11*, 2316. [CrossRef]

Disclaimer/Publisher's Note: The statements, opinions and data contained in all publications are solely those of the individual author(s) and contributor(s) and not of MDPI and/or the editor(s). MDPI and/or the editor(s) disclaim responsibility for any injury to people or property resulting from any ideas, methods, instructions or products referred to in the content.